2023 62nd IEEE Conference on Decision and Control (CDC)
December 13-15, 2023. Marina Bay Sands, Singapore

Propulsion-Free Cross-Track Control of a LEO Small-Satellite Constellation with Differential Drag

Giusy Falcone[1], Jacob B. Willis[1], and Zachary Manchester[1]

***Abstract*— In this work, we achieve propellantless control of both cross-track and along-track separation of a satellite formation by manipulating atmospheric drag. Increasing the atmospheric drag of one satellite with respect to another directly introduces along-track separation, while cross-track separation can be achieved by taking advantage of higher-order terms in the Earth's gravitational field that are functions of altitude. We present an algorithm for solving a multi-satellite formation flying problem based on linear programming. We demonstrate this algorithm in a receding-horizon control scheme in the presence of disturbances and modeling errors in a high-fidelity closed-loop orbital-dynamics simulation. Results show that separation distances of hundreds of kilometers can be achieved by a small-satellite formation in low-Earth orbit over a few months.**

I. Introduction

Formations of multiple satellites are frequently used to perform tasks that a single satellite cannot accomplish alone. Examples include satellite navigation systems, like the global positioning system (GPS), and communications constellations like Iridium and Starlink. The ability to maneuver and control the relative positions of such satellites is key to establishing and maintaining a formation. However, satellites often rely on propulsion systems to maintain these formations, which may be prohibitively large or expensive, especially on smaller spacecraft. Instead, satellites can utilize external perturbation forces to adjust their orbits. In low-Earth orbit (LEO), there are primarily two such forces:

The first perturbation force is atmospheric drag [1], which influences a satellite's altitude and, consequently, its orbital velocity and position. As depicted in Fig. 1, the drag area of a spacecraft can be changed by controlling the attitude of the spacecraft. By placing some spacecraft in a high-drag state and others in a low-drag state, a differential drag between satellites can be introduced and the relative along-track positions of satellites can be changed. This method has been used on orbit to establish and control the along-track positions for constellations of up to 100 satellites [2].

A second perturbation force on LEO satellites is nodal precession [1]. Nodal precession is due to Earth's non-spherical gravity field, and causes orbits to precess, or rotate, around the Earth's polar axis. This effect introduces a small cross-track acceleration on a satellite that varies with altitude. By establishing a large differential altitude between spacecraft, the nodal precession of those spacecraft will occur at different rates, and cross-track orbital changes can be made.

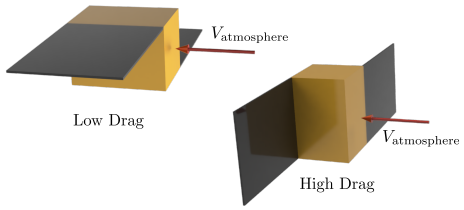

Fig. 1: High- and low-drag configurations for a satellite with attitude-controlled drag modulation.

Most differential-drag formation-flying methods ignore the cross-track influence of nodal precession because it is small compared to the along-track drift, requiring large altitude differences and long time horizons to have a significant effect. This paper introduces a method to leverage nodal precession for long-term differential-drag maneuvers, simultaneously controlling both along-track and cross-track formation shifts. Our contributions include:

- A novel first-order analytical relationship between along-track and cross-track separation changes. This defines a fundamental limit on what along-track and cross-track separations are simultaneously achievable
- A convex trajectory optimization formulation to compute differential-drag sequences that achieve desired formation configurations
- A receding-horizon control strategy that re-plans maneuvers every few orbits to compensate for disturbances and modeling errors
- Simulation results demonstrating our receding-horizon controller performing several different maneuvers in a high-fidelity orbital-dynamics simulation

Throughout the paper we assume the spacecraft is capable of controlling its attitude; this can be performed using a variety of methods including reaction wheels [1] and magnetorquers [3].

The paper proceeds as follows: In Section II we review previous research and on-orbit demonstrations of drag-based formation flying. Section III introduces background concepts that are used in the along-track and cross-track formation flying linear trajectory optimization that we develop in Section IV. The results of a single convex trajectory optimization and closed loop simulations with the trajectory optimization as a feedback controller are shown and discussed in Section V. We conclude in Section VI.

[1]Giusy Falcone, Jacob Willis, and Zachary Manchester are with the Robotics Institute, Carnegie Mellon University, 5000 Forbes Ave., Pittsburgh PA, 15213 {gfalcone, jwillis2, zmanches}@andrew.cmu.edu

II. Related Work

Many studies have explored drag-modulation techniques to enable formation control without propulsion systems. Leonard, et al. first proposed this technique for maintaining the relative separation of spacecraft already in formation [4]. Mathews, et al. [5] investigated a drag-propulsion combination to maintain a cyclical altitude and phase relationship between a spacecraft and a space station. Additional methods have been proposed since then for along-track formation keeping using drag [6]–[9].

Differential drag control for along-track rendezvous has also been studied. Bevilacqua, et al. include J_2 perturbations in their model, which they solve with a two-step analytic method. They do not include cross-track separation in their relative state [10]. Harris and Açıkmeşe [11] propose an optimization approach to differential-drag rendezvous — they use a constrained linear program with minimum-time cost. Most differential-drag methods assume binary drag states where a satellite is in either a low- or high-drag configuration; Harris et al. investigate a continuous drag-modulation scheme based on the coupling of spacecraft attitude and drag [12]. We use a similar continuous-drag formulation, but with an one-norm cost to encourage binary or "bang-bang" drag states.

There have been multiple successful demonstrations of differential-drag control on orbit. The ORBCOMM communications constellation, launched in 1997-1999, used differential drag modulation, along with occasional propulsive maneuvers, to maintain the along-track separation for their network of thirty spacecraft [13]. A limited demonstration of differential drag modulation using deployable panels was performed on-orbit by the AeroCube-4 CubeSat mission in 2012 [14]. Perhaps the most complete on-orbit demonstration of differential drag was for the Planet Earth-imaging constellation [2]. After deployment and initial contact, the slot-allocation and phasing problem was solved by a ground-control system using a genetic algorithm. The CYGNSS constellation also included differential-drag modulation in its mission design [15], and Millenium Space Systems recently demonstrated drag-based station keeping between two satellites on orbit [16].

The Planet differential drag system [2] spawned several derivative works. A continuous optimization of the Planet slot allocation and phasing problem was formulated by Blatner [17]. Repeated updates to handle perturbations, and continuous controls were presented by Sin et al. [18].

All the previously discussed works do not consider cross-track motion of the satellites, and all solutions were computed on the ground. In contrast, our work considers both along-track and cross-track motion, and our control formulation is amenable to autonomous on-orbit implementation.

Two works [19], [20] combine differential drag and nodal precession to modify the cross-track separation of satellites. These works are the most similar to ours. Leppinen [19] performs a feasibility study to demonstrate that differential drag can produce a sufficient altitude separation for nodal precession to change the RAAN of a satellite. No control methods are presented. Lee and Bang [20] present a method for modifying the ground-tracks of satellites in a constellation using differential drag and nodal precession. Synchronization of the along-track and cross-track state of the satellites is not investigated in either of these prior works; this is a key contribution of our work.

We formulate the differential-drag control problem as a convex trajectory optimization problem with a linear cost and linear constraints. Tillerson, et al. solved spacecraft formation flying problems with convex trajectory optimization over twenty years ago [21]. Since that time, convex trajectory optimization has gained popularity for solving many aerospace problems including orbital maneuvering, rocket soft landing, and planetary aerocapture [22], [23].

III. Background

A. Keplerian Motion

A satellite orbiting a perfectly spherical planet with no additional perturbations has dynamics given by the two-body equation:

$$\ddot{\mathbf{r}} = -\frac{\mu}{r^3}\mathbf{r} \tag{1}$$

where $\mathbf{r}$ is the position vector of the spacecraft in the planet-centered inertial frame, $r = \|\mathbf{r}\|$, $\ddot{\mathbf{r}}$ is the acceleration vector, and μ is the planet's standard gravitational parameter.

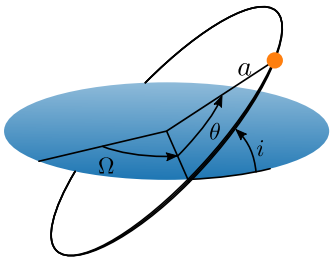

Fig. 2: Notation used to describe the orbital state of a satellite in a circular orbit with the Earth's equatorial plane shown in blue and Ω referenced to an inertially fixed direction.

The orbital state of a satellite is commonly described using the six orbital elements [24]: a, the semi-major axis; e, the eccentricity of the orbit ellipse; i, the inclination; Ω, the right ascension of the ascending node (RAAN); ω, the argument of periapsis; and ν, the true anomaly. In this work, we consider circular orbits, so $e = 0$, and ω and ν are undefined. Instead of ω and ν, we use θ, the argument of latitude (AoL), which measures along-track orbital position from the equatorial plane. In the remainder of this work our focus will be on the dynamics of a, Ω, and θ shown in Figure 2.

A real spacecraft experiences a large number of secondary perturbation forces. The resulting dynamics are

$$\ddot{\mathbf{r}} = -\frac{\mu}{r^3}\mathbf{r} + \mathbf{p}, \tag{2}$$

where $\mathbf{p}$ is the perturbative acceleration vector. The largest perturbation forces on a satellite in LEO are due to atmospheric drag and the Earth's non-spherical gravitational field.

B. Atmospheric Drag

In LEO, atmospheric drag is modeled by

$$\mathbf{D} = -\frac{1}{2m}\rho A C_D v(\mathbf{v} - \mathbf{v_{atm}}) \tag{3}$$

$$\tag{4}$$

where $\mathbf{D}$ is the drag acceleration, ρ is the atmospheric density, A is the satellite's incident cross-sectional area, C_D is the drag coefficient, m is the satellite mass, $\mathbf{v}$ is the inertial velocity vector of the satellite, $\mathbf{v_{atm}}$ is the velocity of the atmosphere, and $v = \|\mathbf{v} - \mathbf{v_{atm}}\|$ is the relative velocity vector magnitude [25], [26]. According to (4), adjusting A through either deployable panels or by changing the spacecraft attitude can modulate drag [2], [27].

Drag always acts in the direction opposing velocity, and can only directly affect the motion of a spacecraft within the orbital plane, decreasing its eccentricity and semi-major axis [28]; since we are assuming circular orbits, we do not consider the eccentricity dynamics due to drag here. This is not a very limiting assumption since drag tends to naturally circularize orbits [29]. The semi-major axis dynamics due to drag are

$$\dot{a} = 2\sqrt{\frac{a^3}{\mu}}D \tag{5}$$

where $D = \|\mathbf{D}\|$ is the magnitude of the drag vector.

C. Nodal Precession and The Method of Averaging

Models of the Earth's gravitational field are typically expressed by a spherical harmonic expansion with coefficients J_n [24], [26]. The first non-spherical term, J_2, is several orders of magnitude larger than all subsequent terms and captures the dominant effect of the Earth's oblateness. Since the J_2 acceleration is rotationally symmetric, it only depends on an orbit's inclination.

On short timescales, the J_2 perturbation impacts all of the orbital elements. However, many of these effects are periodic and average out over an orbit, and only variations on Ω persist over longer time scales. These long-term orbit-averaged dynamics with J_2 can be described by,

$$\dot{\bar{\Omega}} = -\left[\frac{3}{2}\frac{J_2\sqrt{\mu}R_E^2}{a^{7/2}}\right]\cos i \tag{6}$$

$$\dot{\bar{\theta}} = \sqrt{\mu/a^3} \tag{7}$$

where R_E is the Earth's equatorial radius.

IV. Formation Flying

The nodal precession rate and the AoL rate, derived from (6) and (7), demonstrate a dependence on the semi-major axis. Modulating the semi-major axis using drag variation, as shown in (4), facilitates the manipulation of a satellite's AoL and RAAN, enabling the establishment of satellite formations with both along-track and cross-track separations. This section details the linearized dynamics governing the separations between satellites in a formation, and the trajectory optimization approach employed for drag-based formation flying.

A. Linearized Dynamics

We linearize (6) and (7) around a reference semi-major axis a. Similarly, (5) is linearized around a reference drag D, where the satellite's altitude, and thus its atmospheric density and velocity, have been fixed (see Eq. (4)). The resulting linearized equations are:

$$\Delta\dot{\bar{\theta}} = -\frac{3}{2}\sqrt{\frac{\mu}{a^5}}\Delta a \triangleq k_1\Delta a, \tag{8}$$

$$\Delta\dot{a} = 2\sqrt{\frac{a^3}{\mu}}D\Delta D \triangleq k_3\Delta D, \tag{9}$$

$$\Delta\dot{\bar{\Omega}} = \frac{21}{4}J_2\sqrt{\frac{\mu}{a^9}}R_E^2\cos i\Delta a \triangleq k_2\Delta a, \tag{10}$$

where $\Delta\bar{\theta}$, $\Delta\bar{\Omega}$, Δa, and ΔD represent the differences in AoL, RAAN, semi-major axis, and drag force between two satellites, respectively. Notably, from (8) and (10), it's evident that the rates of $\Delta\bar{\theta}$ and $\Delta\bar{\Omega}$ are both influenced by Δa, which implies they cannot be changed independently. Assuming $\Delta\bar{\theta} = \Delta\bar{\Omega} = 0$ initially, all achievable $\Delta\bar{\theta}$ must satisfy

$$\Delta\bar{\Omega} = \frac{k_2}{k_1}\Delta\bar{\theta} \triangleq k_4\Delta\bar{\theta} \tag{11}$$

where $k_4 = k_2/k_1$ is a dimensionless constant that depends only on the reference orbit.

The linear equations (8) to (10) can be put in the standard form of a linear dynamical system,

$$\dot{\mathbf{x}} = A\mathbf{x} + B\mathbf{u}, \tag{12}$$

$$\tag{13}$$

where

$$\mathbf{x} = \begin{bmatrix}\Delta\bar{\theta}\\ \Delta a\end{bmatrix}, A = \begin{bmatrix}0 & k_1\\ 0 & 0\end{bmatrix}, B = \begin{bmatrix}0\\ k_3\end{bmatrix}, \tag{14}$$

and $\mathbf{u} = \Delta D$. We omit $\Delta\bar{\Omega}$ from the state since (11) establishes a relationship between $\Delta\bar{\Omega}$ and $\Delta\bar{\theta}$. The control action, ΔD, is a result of altering the satellite's cross-sectional area exposed to the oncoming atmosphere. In this work, it represents the difference in two spacecraft's attitude between their high- and low-drag configurations, as shown in Fig. 1. When ΔD assumes maximum or minimum values, the two spacecraft have opposite attitude configurations. Conversely, when ΔD is null, it indicates that both satellites maintain identical configurations.

To extend this method to the case of $n > 2$ satellites, one satellite is arbitrarily chosen as the "chief" satellite, and all other satellite's Δ states are referenced to this chief. We concatenate $n-1$ copies of (14) to rewrite (13) as a $2(n-1)$ state system. When referring to the relative state between the chief and another satellite, we use the notation Δa^{1-p} and $\Delta\bar{\theta}^{1-p}$, where p is the index of the satellite.

B. Constraints on the Final Conditions of Drag-Based Formation Control

Given a pair of satellites deployed at the same initial orbit (i.e. $\mathbf{x}_0 = 0$), our goal is to manipulate the differential drag

ΔD over time to achieve a final formation configuration $\mathbf{x}_f$ at some future time t_f. The control strategy involves lowering the orbital altitude of one satellite such that its nodal precession rate is larger than the other satellite. The satellites then remain in this configuration, with $\Delta D = 0$ until a desired $\Delta\bar{\theta}$, and therefore a desired $\Delta\bar{\Omega}$, is achieved. The higher satellite then lowers its altitude to match the first satellite. To maintain a fixed final formation configuration, we must have $\dot{\mathbf{x}}_f = 0$. To satisfy this, (8) to (10) shows that Δa_f and ΔD_f must be zero — the satellites must be at the same final altitude and in the same drag configuration.

Modifying (11) to account for the fact that $\Delta\bar{\theta}$ is an angular quantity, the possible $\Delta\bar{\Omega}$ for a desired final $\Delta\bar{\theta}_f$ are given by

$$\Delta\bar{\Omega}_f = k_4(\Delta\bar{\theta}_f + 2\pi\ell) \tag{15}$$

where ℓ is any integer. To first order, (15) defines the AoL and RAAN separations achievable using drag modulation. For differential-drag formation control to be feasible, (15) is a fundamental limit that must be obeyed when selecting the final $\Delta\bar{\theta}$ and $\Delta\bar{\Omega}$ of a formation.

C. Optimization-Based Drag Maneuver Planning

Given n satellites deployed in the same orbit (i.e., $\mathbf{x}_0 = 0$), we seek to maneuver these satellites into a formation configuration at a final time t_f. To do so with differential drag, we must choose the final state $\mathbf{x}_f$ by choosing the desired value for either $\Delta\Omega_f$ or $\Delta\theta_f$ and selecting the other in accordance to (15). The final altitude or final time are then a result of this choice. It remains to find the necessary control inputs to achieve this formation.

A full trajectory of drag modulation inputs that drives the satellite formation from $\mathbf{x}_0$ to $\mathbf{x}_f$ can be planned by solving the convex optimization problem

$$\begin{aligned}
\underset{\mathbf{x}_{1:N},\,\mathbf{u}_{1:N-1}}{\text{minimize}} \quad & g_f(\mathbf{x}_N) + \sum_{i=1}^{N-1} g(\mathbf{x}_i, \mathbf{u}_i) \\
\text{subject to} \quad & \mathbf{x}_{i+1} = A\mathbf{x}_i + B\mathbf{u}_i, \\
& \left[\Delta a_N^{1-2}, ..., \Delta a_N^{1-n}\right] = 0, \\
& \Delta a_{\min} \leq \left[\Delta a_i^{1-2}, ..., \Delta a_i^{1-n}\right] \leq \Delta a_{\max}, \\
& u_{\min} \leq \mathbf{u}_i \leq u_{\max}
\end{aligned} \tag{16}$$

where $g(x, u)$ is a convex stage cost function, and $g_f(x)$ is a convex terminal cost function. The first constraint enforces the discrete form of the linear dynamics from (13), the second constraint ensures the satellites end at the same final altitude, the third constraint restricts the minimum and maximum altitude differences for each pair of satellites to be within $\Delta a_{\min}$ and $\Delta a_{\max}$, and the final constraint enforces $u_{\min}$ and $u_{\max}$ as lower and upper bounds on the drag achievable by each satellite. In this work, meeting the $\Delta\theta$ final conditions is not treated as a constraint but included in the cost function; this relaxes the problem and avoids infeasibility.

The cost functions g and g_f can be chosen to shape the overall system behavior. To produce minimum-time bang-bang control commands, one-norm costs are used [30]:

$$\begin{aligned}
g_f(\mathbf{x}_N) &= \left\|\Delta\bar{\theta}_N^{1-2} - \Delta\bar{\theta}_f^{1-2}\right\|_1 + ... + \left\|\Delta\bar{\theta}_N^{1-n} - \Delta\bar{\theta}_f^{1-n}\right\|_1 \\
g(\mathbf{x}, \mathbf{u}) &= \left\|\Delta\bar{\theta}^{1-2} - \Delta\bar{\theta}_f^{1-2}\right\|_1 + ... + \left\|\Delta\bar{\theta}^{1-n} - \Delta\bar{\theta}_f^{1-n}\right\|_1 \\
&\quad + \|u_1\|_1 + \|u_2\|_1 + ... + \|u_n\|_1 .
\end{aligned} \tag{17}$$

Other convex cost functions, such as a quadratic costs, are also possible.

V. Simulation Experiments

In our simulation experiments, the linear program in (16) uses (17) as the cost function. Various solvers such as ECOS [31], GLPK [32], or MOSEK [33] can solve it. This work implements (16) and (17) using Julia's Convex.jl modeling toolbox [34] and the MOSEK solver.

The satellite constellation considered consists of identical 1.5kg CubeSats with a $15\text{cm} \times 10\text{cm} \times 10\text{cm}$ chassis and equipped with two deployable solar panels each with dimension $20\text{cm} \times 15\text{cm} \times 0.3\text{cm}$. The satellite's achievable drag ratio is 7.5:1, defined by the equation:

$$D_{ratio} = \frac{D_{max}}{D_{min}} = \frac{A_{max}}{A_{min}}. \tag{18}$$

This ratio quantifies the ability of the satellite to modify drag by adjusting its attitude. Consequently, the input constraints for (16), namely $u_{\min}$ and $u_{\max}$, are set to values of $1/7.5 \approx 0.13$ and 1, respectively.

A. Trajectory Optimization

In this experiment we solve (16) once for a pair of satellites deployed at 440 km altitude and with an inclination of $51.5°$ — conditions that approximate deployment from the International Space Station (ISS). The final conditions are set to $\Delta\bar{\theta}_f = 0$ and $\ell = 2$. From (15), this results in $\Delta\bar{\Omega}_f = 1.4°$, for a maximum cross-track distance of 165 km. In this scenario, the altitude limits, $\Delta a_{\max}$ and $\Delta a_{\min}$, are set to $\pm 10\text{km}$.

The optimization solution for a 1500 orbit time horizon, is in Fig. 3. The top plot shows the drag control trajectory. The bottom three plots show the change in Δa, $\Delta\bar{\theta}$, and $\Delta\bar{\Omega}$ respectively. To increase the relative AoL and RAAN, the orbital altitude of the second satellite is decreased first. The relative AoL increases by $720°$, or two full orbits, and at the end the first satellite lowers its altitude to exactly reach $\Delta\bar{\theta}_f = 0$. The 10km altitude constraint was also satisfied. This optimization took 0.8s to solve on a MacBook Pro with an Apple M1 Pro processor.

B. Closed-Loop Simulation Results

This experiment explores the impacts of realistic modeling errors and disturbances on spacecraft through closed-loop simulations. These simulations integrate additional perturbations not included in (13), including the effects of Earth's rotation on drag, the influence of the first five zonal harmonics (J_1-J_6) for gravity, and an initial orbit eccentricity of $e = 0.005$.

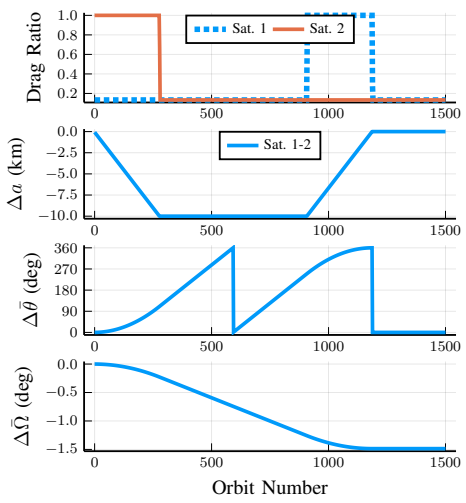

Fig. 3: Optimized trajectory for a two-satellite formation. Top: the drag ratios. Second: the relative altitude. Third: the AoL between the two satellites. Bottom: the RAAN between the two satellites. The satellites end at the same altitude, resulting in a constant final AoL and RAAN.

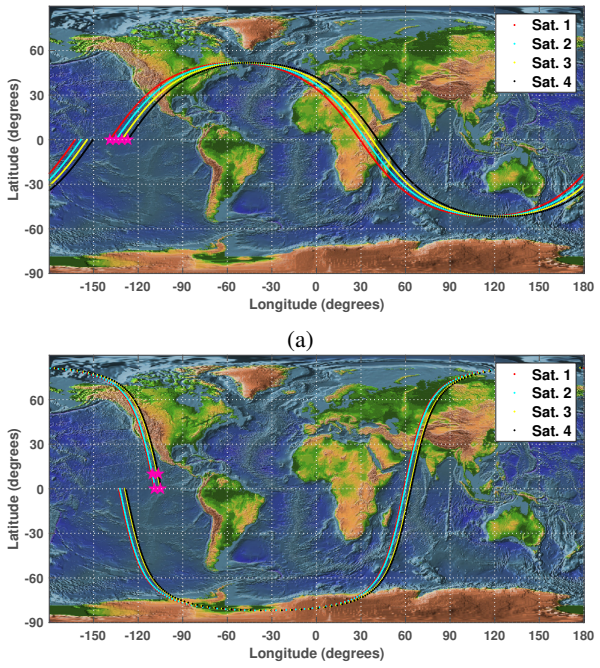

(a)

(b)

Fig. 4: (a) Scenario 1: formation of four satellites in a line with equally distributed RAAN. (b) Scenario 2: formation of four satellites distributed in AoL and RAAN to form the vertices of a square.

To address the challenges posed by modeling errors and disturbances, a model-predictive control (MPC) methodology was employed. This method operates as a receding-horizon loop where, during each iteration, the optimization problem is re-solved using the spacecraft's current measured state. The updated control inputs are then applied until the next iteration. The update frequency of this control loop is once per orbital period. The terminal cost and terminal constraints in (16) ensure the stability of this MPC approach [35].

The receding-horizon control algorithm was applied in two scenarios, depicted in Figs. 4a and 4b and detailed in Sections V-B.1 and V-B.2. The initial state for these scenarios was chosen to emulate common orbits CubeSats are deployed in; due to the ISS and SpaceX Transporter launches. A constant assumption across these scenarios is that all satellites maintain the same drag ratio and start from a uniform state.

1) Scenario 1 — Line Formation: Scenario 1 assumes that four satellites are deployed from the ISS, with an altitude of 440 km, $e = 0.005$, and $i = 51.5°$. The goal is to maneuver the satellites to be equally distributed in the cross-track direction with zero change in AoL, so they pass over the equator in a line, as depicted in Fig. 4a. This corresponds to $\Delta\bar{\theta}_f = 0$ and $\Delta\bar{\Omega}_f = k_4 2\pi\ell$ with $\ell = 1, 2, 3$. In this scenario, the receding-horizon control policy is re-solved once per orbit over a time horizon of 1400 orbits and the altitude limits Δa_{max} and Δa_{min} were set to ± 100 km.

The results of the first scenario are presented in Figs. 5 and 6 and Table I. The final orbit has an altitude of 389.73 km, $e = 0.003$, and $i = 51.477°$. The top plot of Fig. 5 shows the control trajectories for the four satellites. The fourth satellite, the satellite that aims to reach the largest $\Delta\bar{\Omega}$, drives the overall differential drag required for the formation. The bottom plot shows the altitude variation for the four satellites; when the altitude rate is steeper, the satellite is in a high drag configuration. Contrarily, where the altitude rate is shallower, the satellite is in a low drag configuration. Figure 6 shows the AoL and RAAN difference for the three satellite pairs. The difference is calculated with respect to the chief satellite.

Table I reports the overall maneuver time, the final difference in the AoL and the RAAN, and the spherical distance between the chief satellite and the other satellite. It takes three months to reach the final configuration, and the maximum distance between two satellites is 268.3 km.

On average, each optimization took 0.88s to solve on a MacBook Pro with an Apple M1 Pro processor.

Pair	t_f, months	$\Delta\theta_f$, deg	$\Delta\Omega_f$, deg	Spherical Distance, km
Sat. 1 - 2	3	-0.007	-0.75	89.28
Sat. 1 - 3		0.005	-1.5	178.7
Sat. 1 - 4		-0.05	-2.25	268.3

TABLE I: Results for Scenario 1

2) Scenario 2 — Square Formation: The second scenario assumes that four satellites are deployed from an approximately sun-synchronous SpaceX Transporter launch, corresponding to an altitude of 550 km, an $e = 0.005$, and $i = 98°$. The goal is to maneuver the satellites to be distributed in AoL and RAAN to form the vertices of a square, as depicted in Fig. 4b. For this scenario, the ℓ values are 0, 4, and 4, while the $\Delta\bar{\theta}_f$ are 0.03, 0, and 0.03. The

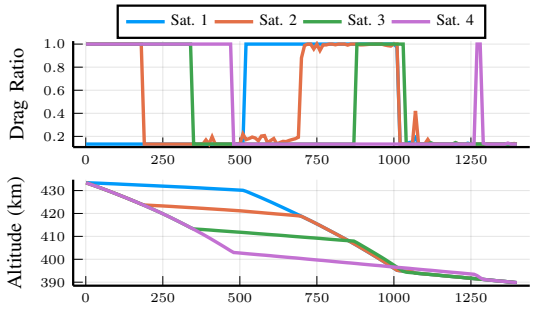

Fig. 5: Scenario 1. Top: The control trajectories for the four satellites. Bottom: The altitude variation of the four satellites. Unlike in Fig. 3, the control trajectories are not piecewise constant due to the on-line correction of disturbances.

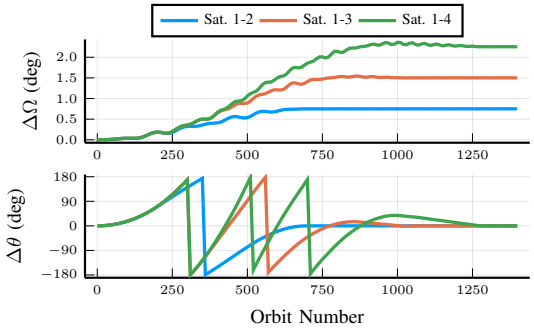

Fig. 6: Scenario 1. Top: RAAN difference with respect to the chief satellite. Bottom: AoL difference with respect to the chief satellite. All the satellite reach the same final AoL.

receding-horizon control policy is re-solved every orbit over a time horizon of 4100 orbits.

Pair	t_f, months	$\Delta\theta_f$, deg	$\Delta\Omega_f$, deg	Spherical Distance, km
Sat. 1 - 2	8.6	10.74	-0.006	1299
Sat. 1 - 3		0.005	-0.63	76
Sat. 1 - 4		10.84	-0.64	1313.5

TABLE II: Results for Scenario 2

The results of scenario 2 are presented in Fig. 7, Fig. 8, and Table II. The final orbit has a 514.1km altitude, e of 0.0043, and i of $98°$. The top plot of Fig. 7 shows the control input, and the bottom plot shows the altitude change for the four satellites. The plots in Fig. 8 report the AoL and RAAN difference for the three pairs. As before, the difference is evaluated with respect to the chief satellite. Table II reports the overall maneuver time, the AoL and RAAN final differences, and the spherical distance between the chief satellite and every other satellite. This scenario takes longer than the first scenario; however, the results show that in less advantageous initial conditions a spacecraft formation with both along-track and cross-track separations can be established using our presented drag-based method. Furthermore, the algorithm is able to define the control trajectory in the presence of disturbances and modeling

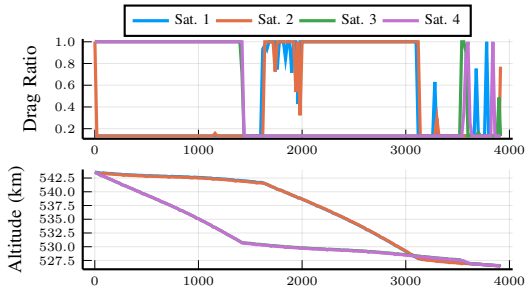

Fig. 7: Scenario 2. Top: The control trajectories for the four satellites. Bottom: The altitude variation of the four satellites. Notice that unlike in Fig. 5, the satellites here change altitude in pairs, with only slight deviations to adjust for the desired AoL difference.

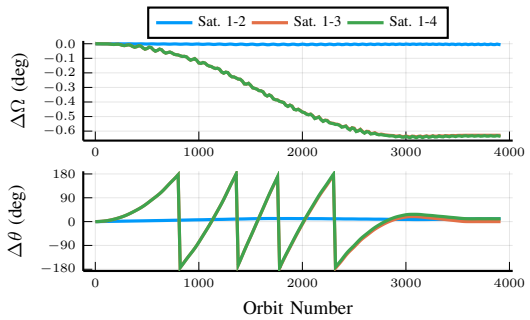

Fig. 8: Scenario 2. Top: RAAN difference with respect to the chief satellite. Bottom: AoL difference with respect to the chief satellite. Satellites 1-2 and satellites 3-4 reach the same RAAN, while satellites 1-4 and satellites 2-3 reach a comparable AoL.

errors. The optimizations took an average of 4.2s each to solve on an Apple M1 Pro MacBook Pro. This took longer than the first scenario due to the extended time horizon.

The two scenarios have interesting differences from a mission-design viewpoint. Lower orbits, like the ISS orbit, result in faster natural orbital decay due to drag, reducing the possible altitude change. However, the lower inclination for the ISS results in a larger k_4 and faster $\Delta\bar{\Omega}$ rate of $0.745°$ per 2π revolution of$\Delta\bar{\theta}$. Contrarily, deployment from the SpaceX Transporter allows a larger available overall altitude change but a smaller $\Delta\bar{\Omega}$ rate of $0.16°$ per 2π revolution of $\Delta\bar{\theta}$. This is why scenario 2 takes longer to complete than scenario 1.

VI. Conclusions

We have presented a novel control scheme that is able to maneuver a low-Earth orbit satellite formation in both along-track and cross-track directions without expending propellant. The drag-based formation control is formulated as a linear program, with solution times of less than one second. This allows it to be used in a receding-horizon manner, updating the control inputs and trajectory for a satellite once per orbit. Simulation results confirm the robustness of the proposed method to disturbances and viability

for autonomous on-orbit implementation. While the scheme assumes known atmospheric density, the actual atmospheric density in low-Earth orbit is widely varying. Future extensions will focus on accurate atmospheric drag estimation, which can be integrated into the trajectory optimization, ensuring robust performance. The proposed approach has the capability to significantly reduce the cost and complexity of deploying multi-plane satellite formations by eliminating the need for propulsion systems onboard.

VII. Acknowledgments

This material is based upon work supported by the National Science Foundation under Grant No. 2111751. A portion of this work was supported by the United States Department of Defense National Defense Science and Engineering Graduate Fellowship (NDSEG).

References

[1] F. L. Markley and J. L. Crassidis, *Fundamentals of spacecraft attitude determination and control*. Springer, 2014, vol. 1286.

[2] C. Foster, J. Mason, V. Vittaldev, L. Leung, V. Beukelaers, L. Stepan, and R. Zimmerman, "Constellation phasing with differential drag on Planet Labs satellites," *Journal of Spacecraft and Rockets*, vol. 55, no. 2, pp. 473–483, Mar. 2018. [Online]. Available: https://arc.aiaa.org/doi/10.2514/1.A33927

[3] A. Gatherer and Z. Manchester, "Magnetorquer-only attitude control of small satellites using trajectory optimization," in *Proceedings of AAS/AIAA Astrodynamics Specialist Conference*, 2019.

[4] C. L. Leonard, W. M. Hollister, and E. V. Bergmann, "Orbital formation keeping with differential drag," *Journal of Guidance, Control, and Dynamics*, vol. 12, no. 1, pp. 108–113, Jan. 1989. [Online]. Available: https://arc.aiaa.org/doi/10.2514/3.20374

[5] M. Mathews and S. Leszkiewicz, "Efficient spacecraft formationkeeping with consideration of ballistic coefficient control," in *26th Aerospace Sciences Meeting*. American Institute of Aeronautics and Astronautics, 1988. [Online]. Available: https://arc.aiaa.org/doi/abs/10.2514/6.1988-375

[6] B. S. Kumar, A. Ng, K. Yoshihara, and A. De Ruiter, "Differential drag as a means of spacecraft formation control," *IEEE Transactions on Aerospace and Electronic Systems*, vol. 47, no. 2, pp. 1125–1135, Apr. 2011.

[7] M. Hunter and S. D'Amico, "Closed-form optimal solutions for propulsive-differential drag control of spacecraft swarms," in *AAS/AIAA Astrodynamics Specialist Conference*, 2022.

[8] S. Varma and K. D. Kumar, "Multiple satellite formation flying using differential aerodynamic drag," *Journal of Spacecraft and Rockets*, Aug. 2012. [Online]. Available: https://arc.aiaa.org/doi/abs/10.2514/1.52395

[9] D. Spiller, F. Curti, and C. Circi, "Minimum-time reconfiguration maneuvers of satellite formations using perturbation forces," *Journal of Guidance, Control, and Dynamics*, vol. 40, no. 5, pp. 1130–1143, May 2017. [Online]. Available: https://arc.aiaa.org/doi/10.2514/1.G002382

[10] R. Bevilacqua and M. Romano, "Rendezvous maneuvers of multiple spacecraft using differential drag under J2 perturbation," *Journal of Guidance, Control, and Dynamics*, vol. 31, no. 6, pp. 1595–1607, Nov. 2008. [Online]. Available: https://arc.aiaa.org/doi/10.2514/1.36362

[11] M. W. Harris and B. Açıkmeşe, "Minimum time rendezvous of multiple spacecraft using differential drag," *Journal of Guidance, Control, and Dynamics*, vol. 37, no. 2, pp. 365–373, Mar. 2014. [Online]. Available: https://arc.aiaa.org/doi/10.2514/1.61505

[12] A. T. Harris, C. D. Petersen, and H. Schaub, "Linear coupled attitude–orbit control through aerodynamic drag," *Journal of Guidance, Control, and Dynamics*, vol. 43, no. 1, pp. 122–131, 2020.

[13] T. Maclay and C. Tuttle, "Satellite stationkeeping of the ORBCOMM constellation via active control of atmospheric drag: operations, constraints, and performance (AAS 05-152)," *Advances in the Astronautical Sciences*, vol. 120, no. 1, p. 763, 2005.

[14] J. Gangestad, B. Hardy, and D. Hinkley, "Operations, orbit determination, and formation control of the AeroCube-4 CubeSats," *Small Satellite Conference*, 2013.

[15] C. D. Bussy-Virat, A. J. Ridley, A. Masher, K. Nave, and M. Intelisano, "Assessment of the differential drag maneuver operations on the CYGNSS constellation," *IEEE Journal of Selected Topics in Applied Earth Observations and Remote Sensing*, vol. 12, no. 1, pp. 7–15, Jan. 2019.

[16] S. Omar, "Drag-based formation control of Millennium Space Systems satellites," *2023 Small Satellite Conference*, 2023.

[17] A. Blatner, "Optimal differential drag control of small satellite constellations," Ph.D. dissertation, University of California at Berkeley, Aug. 2018. [Online]. Available: https://www2.eecs.berkeley.edu/Pubs/TechRpts/2018/EECS-2018-121.pdf

[18] E. Sin, M. Arcak, and A. Packard, "Small satellite constellation separation using linear programming based differential drag commands," in *2018 Annual American Control Conference (ACC)*, Jun. 2018, pp. 4951–4956.

[19] H. Leppinen, "Deploying a single-launch nanosatellite constellation to several orbital planes using drag maneuvers," *Acta Astronautica*, vol. 121, pp. 23–28, Apr. 2016.

[20] J. Lee and H. Bang, "Ground track control using differential drag for small earth observation satellite constellations," *Journal of Spacecraft and Rockets*, vol. 59, no. 5, pp. 1552–1564, 2022.

[21] M. Tillerson, G. Inalhan, and J. P. How, "Co-ordination and control of distributed spacecraft systems using convex optimization techniques," *International Journal of Robust and Nonlinear Control: IFAC-Affiliated Journal*, vol. 12, no. 2-3, pp. 207–242, 2002.

[22] X. Liu, P. Lu, and B. Pan, "Survey of convex optimization for aerospace applications," *Astrodynamics*, vol. 1, pp. 23–40, 2017.

[23] D. Malyuta, Y. Yu, P. Elango, and B. Açıkmeşe, "Advances in trajectory optimization for space vehicle control," *Annual Reviews in Control*, vol. 52, pp. 282–315, 2021.

[24] H. D. Curtis, *Orbital Mechanics for Engineering Students*, 3rd ed. Elsevier Butterworth Heinemann, 2005, p. 652–715.

[25] J. E. Prussing and B. A. Conway, *Orbital Mechanics*. Oxford University Press, 2013, ch. 9. Perturbation, p. 155–168.

[26] V. A. Chobotov, *Orbital Mechanics*. American Institute of Aeronautics and Astronautics, Inc., 2002, ch. 8. Introduction to Orbit Perturbations, p. 185–213.

[27] G. Falcone and Z. R. Putnam, "Energy depletion guidance for aerobraking atmospheric passes," *Journal of Guidance, Control, and Dynamics*, vol. 45, no. 4, pp. 651–668, 2022.

[28] J. R. Wertz, *Space mission analysis and design*. Microcosm Press, 2005, ch. 6. Introduction to Astrodynamics, p. 131–159.

[29] J. A. Burns, "Elementary derivation of the perturbation equations of celestial mechanics," *American Journal of Physics*, vol. 44, no. 10, pp. 944–949, Oct. 1976. [Online]. Available: http://aapt.scitation.org/doi/10.1119/1.10237

[30] L. Zadeh and B. Whalen, "On optimal control and linear programming," *IRE Transactions on Automatic Control*, vol. 7, no. 4, pp. 45 – 46, 1962.

[31] A. Domahidi, E. Chu, and S. Boyd, "ECOS: An SOCP solver for embedded systems," in *2013 European control conference (ECC)*. IEEE, 2013, pp. 3071–3076.

[32] A. Makhorin, "GLPK (GNU linear programming kit)," https://github.com/jump-dev/GLPK.jl, 2023.

[33] ApS MOSEK, "The MOSEK optimization software," https://github.com/MOSEK/Mosek.jl, 2021.

[34] M. Udell, K. Mohan, D. Zeng, J. Hong, S. Diamond, and S. Boyd, "Convex optimization in Julia," *SC14 Workshop on High Performance Technical Computing in Dynamic Languages*, 2014.

[35] D. Q. Mayne, J. B. Rawlings, C. V. Rao, and P. O. Scokaert, "Constrained model predictive control: Stability and optimality," *Automatica*, vol. 36, no. 6, pp. 789–814, 2000.